Materials Research Proceedings **13** (2019) 85-90 https://doi.org/10.21741/9781644900338-15

FTMP-Based Quantitative Evaluations for Dynamic Behavior of Dislocation Wall Structures

Shiro IHARA[1, a *], Tadashi HASEBE[1,b]

[1]1-1, Rokkodai-cho, Nada-ku, Kobe, Hyogo, Japan

[a]ihara.shiro@mail.mm4.scitec.kobe-u.ac.jp, [b]hasebe@mech.kobe-u.ac.jp

Keywords: Dislocation, Crystal Plasticity, Field Theory, Differential Geometry, Dislocation Dynamics

Abstract. Field theory of multiscale plasticity (FTMP) is applied to the quantitative evaluations of geometrically necessary boundaries (GNBs) of dislocations. Reproduced four representative GNBs via dislocation dynamics simulations are scrutinized via the duality diagram representation scheme and the Shannon entropy. Notable correlations are found both between the entropy and the incompatibility, and the mean entropy rate and the incompatibility rate. Furthermore, the mean entropy rate is linearly correlated also with the log of the incompatibility. Combined with a unified correlation for all the GNBs on the duality diagram, we demonstrate the effectiveness of the FTMP-based stability/instability criterion proposed in the previous study.

Introduction

Evolving dislocation substructures are one of the key features in achieving practically-feasible multiscale modeling of crystalline metallic materials. Geometrically necessary boundaries (GNBs) of dislocations[1,2] are classified as the typical wall structures among others that play pivotal roles not only for determining mechanical responses but also for controlling recrystallization processes[2,3]. For dealing with these, however, the widely-recognized dislocation density tensor, or equivalently, the concept of geometrically-necessary dislocations [4], seem to be incompetent, for it vanishes when counting both-signed components of dislocations simultaneously. This shortcoming brings about serious problems in tackling dislocation ensembles in general. The incompatibility tensor, on the other hand, has been demonstrated to readily and effectively solve those issues when it is appropriately utilized in the context of Field Theory of Multiscale Plasticity (FTMP) [5]. The theory relates the quantity with the energy-momentum tensor fluctuation after extended to 4D space-time [5], providing us with a new perspective regarding the quantity as the underlying microscopic degrees of freedom that plays critical roles as the destinations of excessively stored strain energy during the course of elasto-plastic deformations.

The present study targets four representative GNBs, whose detailed structures have been identified by Winther et al. [1]. The GNBs are reproduced by using dislocation dynamics method and the processes as well as the obtained configurations are evaluated based on FTMP, in particular, via duality diagram representations. We further characterize the simulated dislocation configurations by the Shannon entropy [6], and attempt to extensively examine in detail the organic interrelationships that can be expected to exist between the two quantities.

Theoretical Background

According to the non-Riemannian geometry, all the imperfections in crystalline materials space are completely represented by combinations of the torsion and the curvature [5]. The former is defined as the closure failure of the circuit around the defected field, while the latter is characterized by the rotation of the material vector after its parallel displacement along the

circuit. From the definition, they correspond to the dislocation density tensor and the incompatibility tensor, respectively.

The incompatibility tensor η_{ij}can be obtained as the spatial curl against the dislocation density tensor α_{ij} as,

$$\eta_{ij} = -\epsilon_{i|kl|}(\partial_{|k|}\alpha_{jl}) \tag{1}$$

In this study, we evaluate the dislocation density tensor$\boldsymbol{\alpha}$based on the following equation.

$$b_l = \int_s \ \alpha_{jl} \ \mathrm{d}S_j \tag{2}$$

Here, b_l is the Burgers vector and $\mathrm{d}S_j$is the surface through which dislocation lines penetrate. We once obtain α_{ij} by dividing simulation cells into a prescribed number of sub-cells, and calculate the spatial derivatives.

In FTMP, presuming that incompatible displacements are driven by the inhomogeneous forces acting on them (flow-evolutionary hypothesis) [5], we derive the relationship between the incompatibility tensor and the fluctuation part of energy-momentum tensor δT_{ij}as,

$$\eta_{ij} = \kappa\delta T_{ij}, \tag{3}$$

where κ represents the duality coefficient, which is a sort of the transport coefficient,δmeans the deviation from the spatio-temporal average, and the subscripts *i* and *j* denote four-dimensional spatio-temporal components, i.e., *i, j* = 1, 2, 3, and 4.Considering the temporal components for the both tensors, we have a relationship between the incompatibility and the energy fluctuation, as follows.

$$\eta_{KK} = \kappa(\delta U^e + \delta K), \tag{3'}$$

where $U^e$is the elastic strain energy and $K$is the kinetic energy. In this study, K is defined as

$$K = \frac{1}{2}\rho b^3 l v^2, \tag{4}$$

where $\rho$is the density, b is the magnitude of Burgers vector, $l$is the segment length and $v$is the speed of dislocation nodes. In the static problem, K can be neglected. By plotting the two quantities in Eq.(3'), we obtain the duality diagram, allowing us to visualize the energy flow into the incompatibility-based degrees of freedom, accompanied by configurational changes occurring in the targeted dislocation systems.

The Shannon entropy $S_S^{config}$is evaluated as follows [6,7],

$$S_S^{config} = -\sum f_i \log f_i \tag{5}$$

Here,$f_i$is defined as the length ratio of the dislocation segments for the sub-cell *i*, i.e., the segment length of the dislocations contained in the sub-cell *i* divided by the total length within the simulation cell. Note that the commonly-used definition based on the number of points is not suitable in the present context, because the "number" varies as a function of the curvature of the segment independent of the segment length during the simulations.

Simulation Conditions and Results

After producing four representative GNBs [8], i.e., GNB2, 3, 4 and7, which has been identified and classified by Winther, et al. [1], we examine the formation processes based on the duality diagram representation scheme in the following.

Figure 1 summarizes the simulation results, displaying the initial and the final configurations, each compared with the ideal counterpart by Winther, et al. [1]. The GNB2 ultimately yields a regular hexagonal network, as shown in Fig.1, while relatively complex configurations accompanied by crooked segments are resulted for the GNB4. Mutually similar final configurations consisting basically of straight segments, on the other hand, are obtained for the GNBs 3 and 7. Generally, we confirm good agreements between the ideal morphologies and the corresponding simulated final configurations. To be noted that slightly curved segments in the simulated GNB4 are due to the residual internal stress field, not completely screened out even in the terminal state because of its highest dislocation density among others.

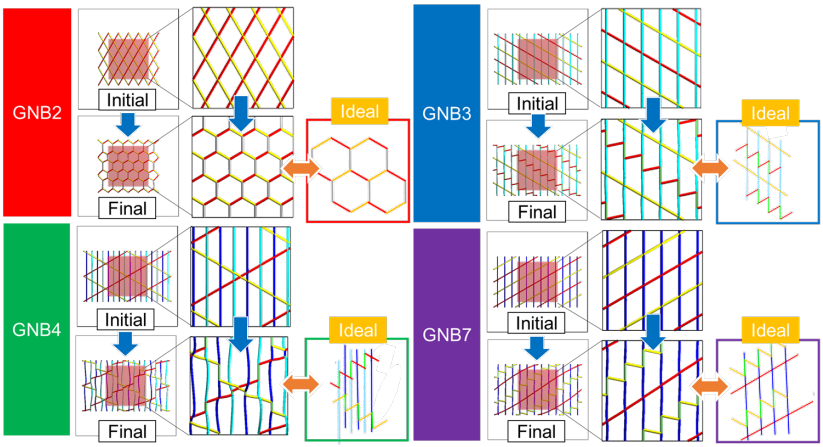

Fig.1 Simulated initial and final configurations for GNBs 2, 3, 4 and 7, compared with those predicted by Winther, et al [1].

Figure 2 displays duality diagrams for the above formation processes for the four GNBs, (a)without and (b)with considering the virtually-enhanced contributions of the kinetic energy fluctuation δK(eq.(3')), where the final states are indicated by solid symbols. The multiplying factor employed here is $\alpha = 1 \times 10^7$. As demonstrated in Fig.2(a), we find a unified trend governing all the GNBs: all the final states tend to align on a single master curve in the diagram. The virtual contributions of δK in Fig.3(b), on the other hand, indicate the rate of the configurational changes toward the final states, with the GNB2 exhibits the maximum, the GNB3 and 7 the intermediate, and the GNB4 yields the minimum, from which we can conclude the following. The GNB2 tends to reach its final configuration quite rapidly compared to others, as schematically illustrated in the insets in Fig.3(b) via rolling-down ball in steeper energy landscape.

The authors [8] proposed a new stability/instability criterion based on the above observations, as overdrawn on Fig.3(a), where the relationships between the disturbances$\Delta(\delta U^e)$ and the corresponding configurational changes measured by $\Delta\eta_{KK}$ for the GNB2 and GNB4 are indicated. The most stable GNB2 tends to cope with such disturbances by its relatively large configurational changes, whereas the GNB4 tries to withstand them rather firmly with minimum morphological variations. The above result about the virtual contributions ofδKsupports this postulate.

Materials Research Proceedings **13** (2019) 85-90 https://doi.org/10.21741/9781644900338-15

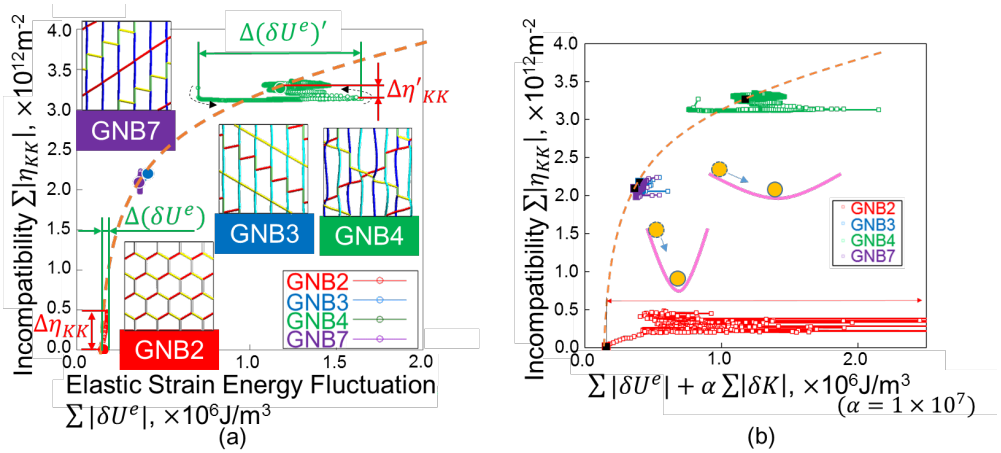

Fig.2 Duality diagrams for simulated GNBs (a) without and (b) with virtually enhanced contribution of kinetic energy term.

Relationships with Shannon Entropy

Since the Shannon entropy counts for the configurational information by nature, one can expect some correlations between what are to be represented by the quantity and the incompatibility discussed above.

Figure 3(a) shows the variation of the evaluated entropy with elapsed time for the four GNBs. The GNB2, with regular hexagon as the final configuration, exhibits the minimum entropy, together with the largest drop rate, while the GNB4, with the most complex configuration as well as the highest dislocation density among the four, yield the maximum value with the minimum mean decreasing rate, following relatively large temporal fluctuations. The GNBs 3 and 7, on the other hand, tend to converge to mutually similar values at the final configurations, simply because they basically have the same configuration. Figure 3(b) is the same plot as Fig.3(a) but for the incompatibility, from which we notice similar overall varying trend to that for the entropy. To further examine the similarity, we plot the entropy with the incompatibility in Fig.4(a). As expected, we confirm roughly a linear correlation between the two, where the trend seems to hold for both the initial and the final states, i.e.,

$$S_S^{config} = k^{config}\eta_{KK} \tag{6}$$

This strongly implies the incompatibility tensor contains also the features measured by the entropy, in particular, those about the configurational details.

Plotting the average rates of the two quantities, i.e., $\langle S_S^{config}\rangle_t^{\cdot}$ with $\langle \eta_{KK}\rangle_t^{\cdot}$ as shown in Fig.4(b), we also have a linear relationship between the two. Here, $\langle\ \ \rangle_t^{\cdot}$denotes the temporal average over the elapsed time until reaching each final configuration. This, together with the linear correlation between $S_S^{config}$and η_{KK}in Fig.4(a), implies,

$$\langle S_S^{config}\rangle_t^{\cdot} = k^{config}\langle \eta_{KK}\rangle_t^{\cdot} \tag{7}$$

with k^{config} representing the same coefficient as in Eq.(6).

Furthermore, we findsimilar trends also in the order of the mean decreasing rates $\langle S_S^{config}\rangle_t^{\cdot}$in Fig.3(b) and that of the magnitude of η_{KK}in Fig.3(b). In this regard, we additionally examine the relationship between the mean entropy rate and the incompatibility. Figure 5displays the plot of $\langle S_S^{config}\rangle_t^{\cdot}$ versus η_{KK}on the semi-log basis. The mean entropy rate is demonstrated to be well

correlated also with the incompatibility both at the initial and final states, which is equated as follows, i.e.,

$$\langle S_S^{config} \rangle_t = k_{\ln}^{config} \ln \eta_{KK} \tag{8}$$

The relarionship between Eqs.(7) and (8) deserves further investigations.

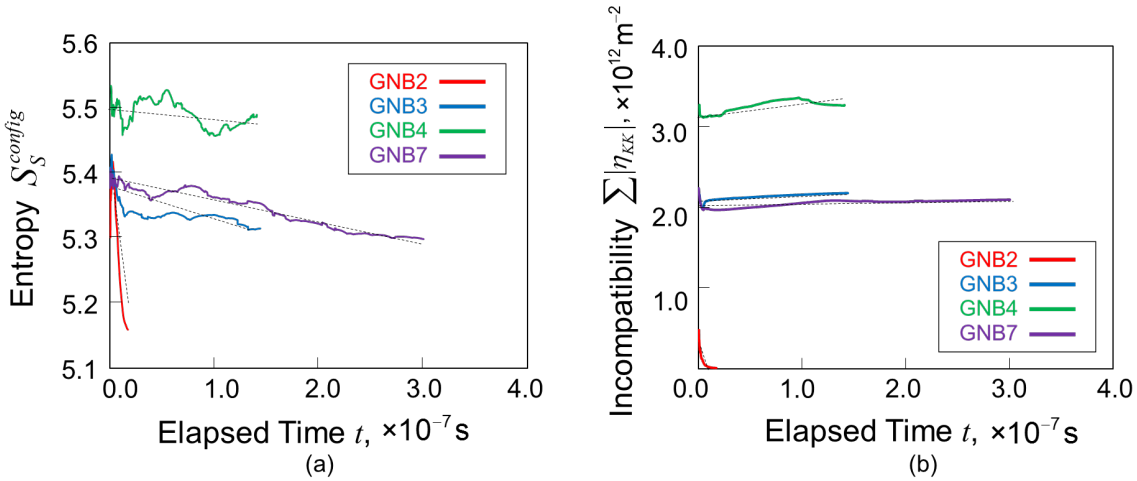

Fig.3 Variations of (a)entropy and (b) incompatibility for four GNBs.

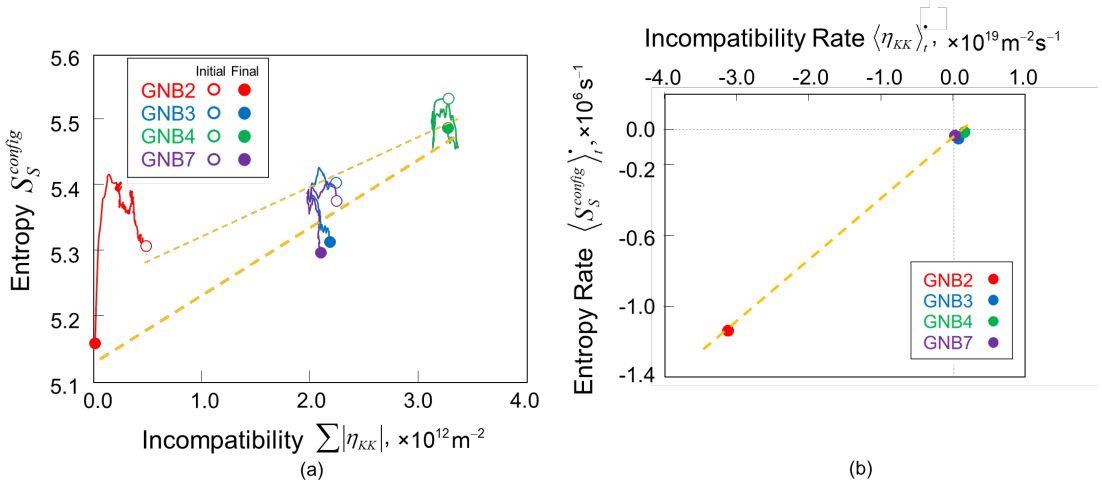

Fig.4 Relationships (a) between entropy and incompatibility and (b) between entropy rate and incompatibility rate.

Let us remind here the readers the flow-evolutionary hypothesis given by Eq.(3'), where the incompatibility is to be driven by the energy fluctuations. Since the entropy rate governs the rate of patterning in general, the linear relationships in Fig.4(b) and Fig.5 means that the dislocation patterning into GNBs is controlled by the energy fluctuations of the targeted systems.

In summary, those demonstrated above can provide a strong leverage that supports effectiveness of the duality diagram-based stability criterion proposed in [8], together with the critical roles played by the incompatibility tensor as the mediator for substantial understanding of the GNBs.

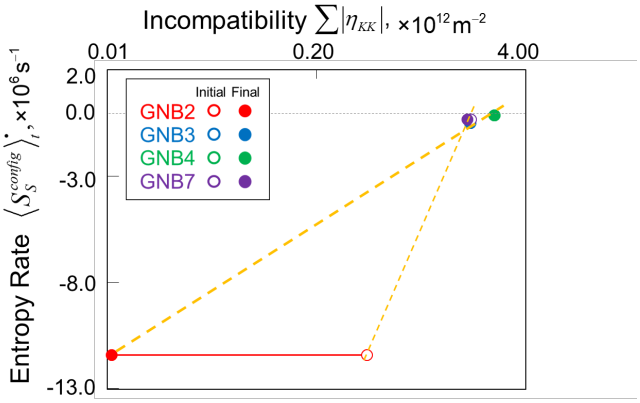

Fig.5 Relationships between entropy rate and log of incompatibility.

Summary

After briefly describing the FTMP-based evaluation against the four typical GNBs in the light of the duality diagram representation scheme, we further examine their configurational aspects based on the Shannon entropy. Extensive comparisons are made with the incompatibility tensor-based counterparts. The direct comparison of the two eloquently demonstrates that this simple conjecture seems to be effective, although its generality must be further examined. This finding also provides a leverage that strongly supports the duality diagram-based stability/instability criterion proposed in the previous study.

References

[1] G. Winther, C. Hong, and X. Huang, Low-Energy Dislocation Structure (LEDS) character of dislocation boundaries aligned with slip planes in rolled aluminium, Phil. Mag. 95 (2015) 1471-1489. https://doi.org/10.1080/14786435.2015.1033488

[2] N. Hansen, Deformation microstructures with a structural scale from the micrometre to the nanometre dimension, Evolution of Deformation Microstructures in 3D, Eds.Gundlach, C., et al. (Proc. 25th Riso Int. Symp Maters.Sci.) (2004) 13-32.

[3]O. V. Mishin, A. Gofrey, D. Juul Jensen and N. Hansen, Recovery and recrystalizaion in commercial purity aluminum cold roled to an ultrahigh strain, Acta Mater. 61 (2013) 5354-5364. https://doi.org/10.1016/j.actamat.2013.05.024

[4] Fleck, N.A., and Hutchinson, J.W., 2001, A reformulation of strain gradient plasticity, J. Mech. Phys. Solids 49, 2245-2271. https://doi.org/10.1016/s0022-5096(01)00049-7

[5]T. Hasebe, M. Sugiyma, H. Adachi, S. Fukutani, and M. Iida, Modeling and simulations of experimentally-observed dislocation substructures based on Field Theory of Multiscale Plasticity (FTMP) combined with TEM and EBSD-Wilkinson method for FCC and BCC poly/single crystals, Mater. Trans. 55 (2014)779-787. https://doi.org/10.2320/matertrans.m2013226

[6]Shannon, C.E., A mathematical theory of communication, Bell Syst. Tech. J. 27 (1948) 379-423.

[7] A.M. Hussein and J. A. El-Awady, Quntifying dislocation microstructure evolution and cyclic hardeining in fatigued face-centered cubic single crystals, J. Mech. Phys. Solids 91 (2016) 126-144. https://doi.org/10.1016/j.jmps.2016.03.012

[8]S. Ihara and T. Hasebe, FTMP-based simulations and evaluations of Geometrically-Necessary Boundaries (GNBs) of dislocation, *Model. Simul. Mater. Sci.* (Submitted) (2019).